Electronic Supplementary Material (ESI) for Nanoscale.

Supporting information of

Intermetallic Pd-Y Nanoparticles/N-doped Carbon Nanotubes as Multi-active Catalysts for Oxygen Reduction, Ethanol Oxidation, and Zinc-air Battery

Nipa Roy[a,b], Mohammad Shamsuddin Ahmed[c,d], Hyo Kyoung Lee[e], Seungwon Jeon[a†]

[a]Department of Chemistry and Institute of Basic Science, Chonnam National University, Gwangju 500-757, Republic of Korea. Tel.: +82 62 530 0064; Fax: +82 62 530 3389

[b]Department of Physics, Yeungnam University, Gyeongsan 38541, Republic of Korea

[c]Institute of Energy Studies, University of North Dakota, Grand Forks, North Dakota, United States 58202

[d]Department of Materials Science and Engineering, Chonnam National University Gwangju 61186, Republic of Korea

[e]School of Architecture, Chosun University, 309 Pilmun-daero, Dong-gu, Gwangju, 61452, Republic of Korea

†Corresponding author: Name: Seungwon Jeon; Email: swjeon3380@naver.com

1. Experimental details

1.1. Chemicals and reagents

Single-walled CNTs with an average tube diameter of 20–30 nm and length of 1–2 µm were obtained from Carbon NanoTech. Co., Ltd., South Korea. 1,5-NDA, yttrium (III) nitrate hexahydrate ($Y_2(NO_3)_3 \cdot 6H_2O$), potassium tetrachloropalladate (II) (K_2PdCl_4), and sodium borohydride ($NaBH_4$) were purchased from Sigma–Aldrich, Korea. Sulfuric acid and nitric acid were procured from Ducksan Pure Chemical Industries Co., Ltd. Methanol, ethanol, potassium hydroxide, and potassium chloride were purchased from Dae-Jung Co., Korea. All chemicals and reagents were used of analytical grade and were used without further purification.

1.2. Instruments

A three-electrode configuration comprising a reference electrode (Ag/AgCl in a 3.0 M KCl filling solution), a counter electrode (Pt wire), and a working electrode (glassy carbon electrode, GCE) with a uniform diameter of 3.0 mm was employed. To perform electrochemical analysis, we conducted cyclic voltammetry, linear sweep voltammetry, and chronoamperometry using a grounded three-electrode potentiostat in a Faraday cage. Moreover, an electrochemical workstation (CHI700C) and a rotating ring-disk electrode (RRDE) method (EG & G Model 636) were used for hydrodynamics. pH was accurately adjusted using a pH glass electrode with a JENCO meter. High-resolution transmission electron microscopy (TEM) and energy-dispersive X-ray spectroscopy (EDX) were performed on a JEM-2100F microscope (200 kV). X-ray photoelectron spectroscopy (XPS) was conducted using a MultiLab 2000 instrument (Thermo Electron Corporation, England) with an Al Kα X-ray source and an energy of 14.9 keV. Furthermore, inductively coupled plasma atomic emission spectroscopy (ICP-AES) was used to determine the weight percentage of metal elements in the synthesized PdY/NCNTs nanostructure. X-ray diffraction (XRD) patterns and Raman spectra of the three samples were obtained from a Rigaku D/max-2500 instrument and a LabRam HR800 UV Raman microscope (Horiba Jobin-Yvon, France) using an Ar^+ laser with 515 nm excitation, respectively.

K-L equation

$$\frac{1}{j} = \frac{1}{j_k} + \frac{1}{j_L} = \frac{1}{j_k} + \frac{1}{B\omega^{1/2}} \qquad (1)$$

$$B = 0.62\,\eta F A C_{O_2} D_{O_2}^{2/3} V^{-1/6} \qquad (2)$$

where j is the experimentally measured current density; j_k and j_l are the kinetic and diffusion limiting current densities (mA/cm^2), respectively; ω is the angular velocity of the disk ($\omega = 2\pi$ rpm); A and η are the surface area of the disk and electron transfer number, respectively; T and F are the temperature and Faraday constant (96485.2 C mol^{-1}), respectively; C_{O_2} and D_{O_2} are the concentration (1.2 mM L^{-1}) and diffusion coefficient (1.9×10^{-5} cm^2 S^{-1}) of dissolved O_2 in 0.1 M KOH, respectively; and V is the kinetic viscosity of the electrolyte (1×10^{-2} cm^2 S^{-1}. Based on the K–L equation, plots of j^{-1} vs. $\omega^{1/2}$ were analyzed at various electrode potentials. These plots yielded a straight line, and the slopes of these plots reflected the B factor in equation (1).

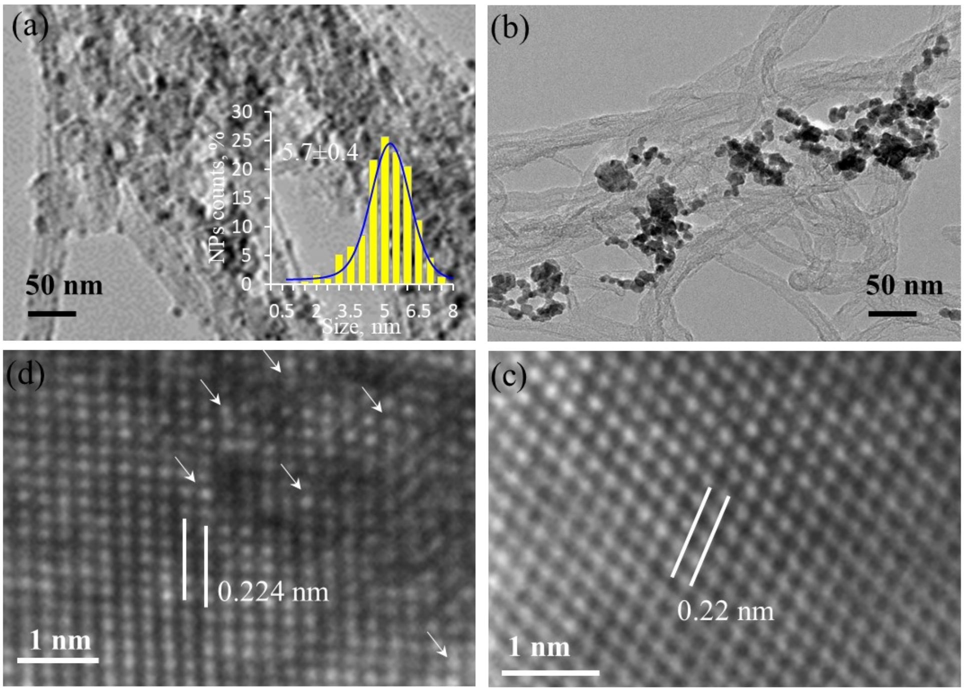

Figure S1: TEM images of pure Pd/NCNTs (a) PdY/CNTs (b) and HRTEM image of Pd/CNTs (c) and PdY/NCNTs (d), inset: the Pd NPs size dependent histogram.

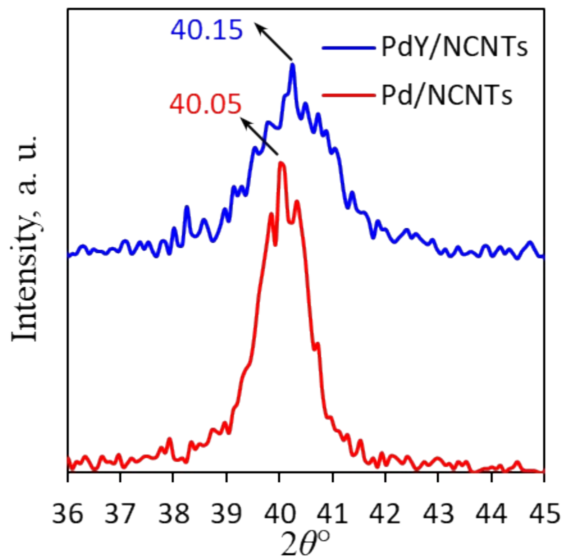

	FWHM	K	Lamda	theta	Particle size
Pd/NCNTs	1	0.897	0.1541	40.05	8.43
PdY/NCNTs	1.61			40.15	5.24

Figure S2: The enlarged XRD pattern at (111) plan of FCC Pd and the corresponding parameters used in the calculation.

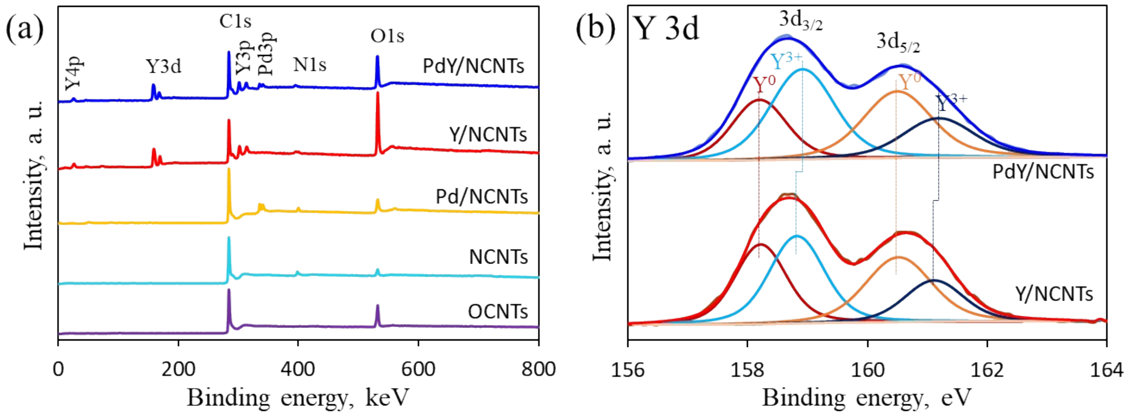

Figure S3: XPS survey spectra of corresponding samples (a) and core level of Y 3d XPS spectra of PdY/NCNTs and Y/NCNTs (b).

Table S1: Elemental composition of all samples data obtained from the area of XPS peaks.

	C wt%	O wt%	N wt%	Y wt%	Pd wt%
OCNTs	66.1	33.9	-	-	-
NCNTs	60.2	25.8	14	-	-
Pd/NCNTs	68.9	10.2	9		11.9
Y/NCNTs	69.3	11.4	8.9	10.4	
Pd/CNTs	74.5	8.9	-	-	16.6
PdY/NCNTs	61.2	8.6	7	10.1	13.1

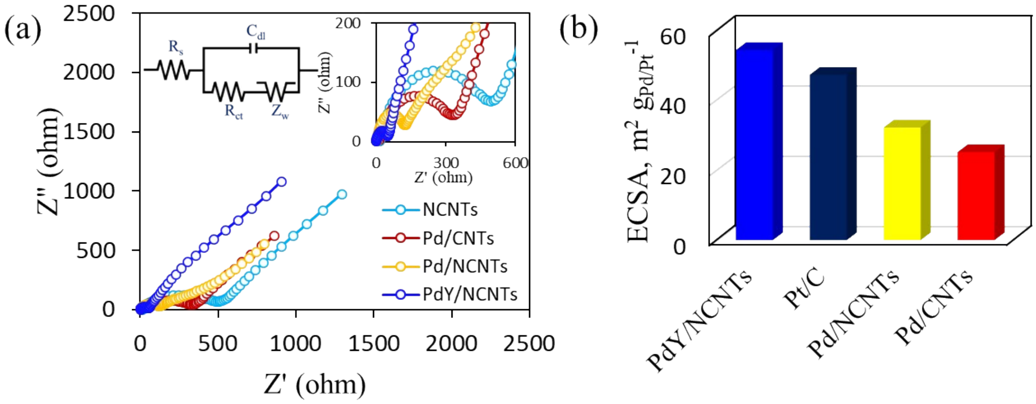

Figure S4: EIS spectra of electrocatalysts recorded in an Ar-saturated 0.1 M KCl containing 5 mM $Fe(CN)_6^{3-/4-}$ solution at a frequency range from 10^6 to 10^{-2} Hz (a); insets: enlarged EIS spectra and the equivalent circuit model, the comparison of ECSA calculated from the CV curves (b).

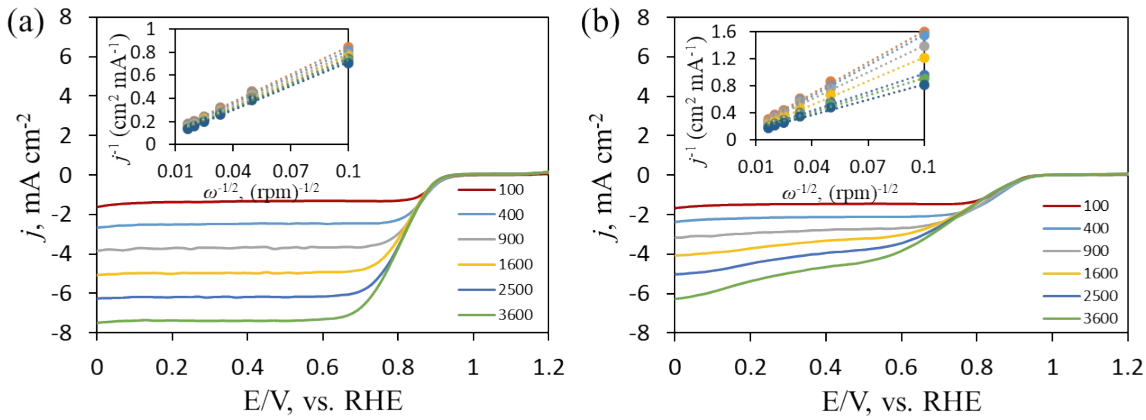

Figure S5: LSV curves at various speed ranges for Pd/NCNTs (a) and Pd/CNTs (b); insets: corresponding K–L plots at a potential range of 0.0 to 0.6 V (vs. RHE).

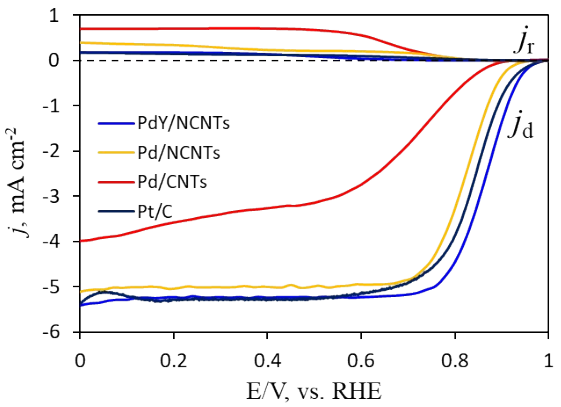

Figure S6: RRDE curves for ORR at 1600 rpm in respect to the variable potential from 1.0 to 0.0 V (vs. RHE) on disk electrode and a constant applied potential of 0.8 V (vs. RHE) on the ring electrode.

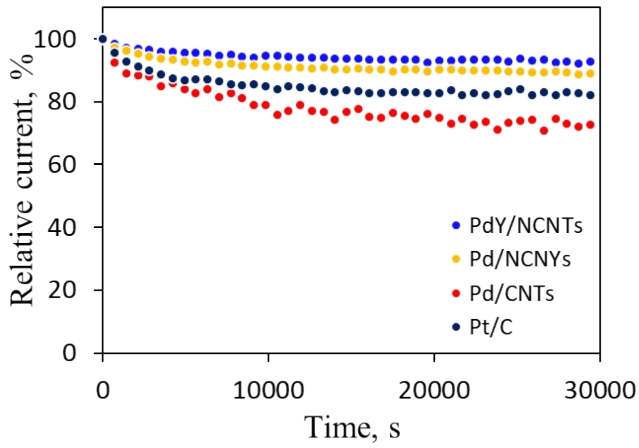

Figure S7: CA curves of all Pd-containing catalysts and Pt/C in O_2-purged 0.1 M KOH electrolyte at a constant applied potential of 0.8 V (vs. RHE).

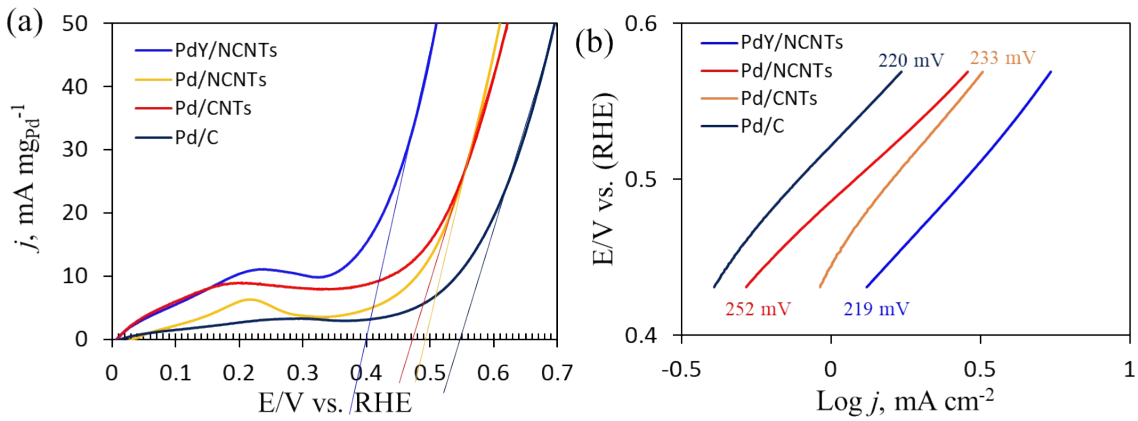

Figure S8: Enlarged CV curves of EOR at E_0 region (a) and Tafel plots (b) of all Pd-loaded catalysts.

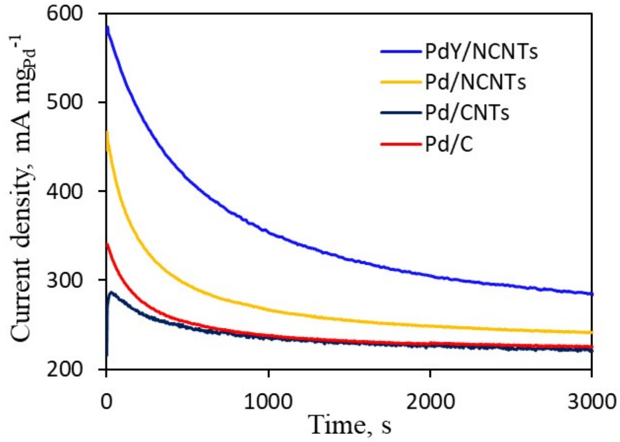

Figure S9: CA curves of all Pd-containing catalysts at j_f of PdY/CNTs (0.92 V vs. RHE) in Ar-purged 1 M KOH electrolyte containing 0.2 M ethanol.

Table S2: Comparison of PdY/NCNTs with recently reported Pd-based catalysts in respect to the ORR performance.

Materials	Electrolyte	E_0 (V vs. RHE)	$E_{1/2}$ (V vs. RHE)	MA (mA mg_{Pd}^{-1}) $^{@\sim E1/2}$	SA (mA cm^{-2})	Refs.
PdY/NCNTs	0.1M KOH	0.98	0.865	1317	16.775	This work
CPCo-3	0.1M KOH	0.932	0.886	-	17.08	[S1] 2023
$Sn_{18}Pd_{82}$ alloys	0.1 M KOH	1.05	0.92	2300	3.46	[S2] 2023
Pd@CoOx/NC1	0.1 M KOH	1.07	0.95	280	3.7	[S3] 2023
N-10h-$Pd_3P_2S_8$	0.1 M KOH	0.9	0.76	760	0.45	[S4] 2022
Pd/FeCoNC	0.1 M KOH	0.95	0.86	-	-	[S5]2022
P-PdPb NFs	0.1 M KOH	1.06	0.95	130	9.2	[S6]2022
Pd NBs/C	1 M KOH	0.99	0.95	1210	3.6	[S7]2021
PdBi_8h	0.1 M KOH	0.99	0.93	180	5.3	[S8]2021
PdY nanosponges	0.1 M KOH	1.02	0.90	4.00#	7.98	[S9] 2023
Au@Pd NWs	0.1 M KOH	-	0.927	910	1.3	[S10] 2023
PdZn bimetallene	0.1 M KOH	1.13	1.05	1.11#	2.16	[S11] 2023

*mA/cm_{Pd}^2; # mA μg_{Pd}^{-1}

References

[S1] T. Yang, D. Bhalothia, H. W. Chang, C. Yan, A. Beniwal, Y. X. Chang, S. C. Wu, P. C. Chen, K. W. Wang, S. Dai, T. Y. Chen, Oxygen vacancies endow atomic cobalt-palladium oxide clusters with outstanding oxygen reduction reaction activity, Chem. Eng. J. 454 (2023) 140289

[S2] D. Liu, S. Tian, Y. Zhang, C. Hu, H. Liu, D. Chen, L. Xu, and J. Yang, Ultrafine SnPd nanoalloys promise high-efficiency electrocatalysis for ethanol oxidation and oxygen reduction, ACS Appl. Energy Mater 6 (2023) 1459−1466.

[S3] F. Nasim, H. Alia, M. A. Nadeem, The pronounced effect of cobalt oxide on the electrocatalytic activity of palladium nanoparticles anchored on CoOx/NC towards the ORR with increased MA and ECSA, Mater. Adv., 2023, 4, 578–585.

[S4] S. W. Koh, J. Hu, H. Chun, P. Yu, J. Ge, Z. Sun, W. Hong, Q. Liu, K. Nam, B. Han, Z. Liu, H. Li, Two-Dimensional Palladium Phosphoronitride for Oxygen Reduction, ACS Appl. Mater. Interfaces 14 (2022) 12156−12167.

[S5] Z. Cui, X. Bai, Highly active and stable Fe/Co/N Co-doped carbon-anchored Pd nanoparticles for oxygen reduction reaction, ACS Appl. Mater. Interfaces, 14 (2022) 9024−9035.

[S6] Z. Wang, P. Tian, H. Zhang, K. Deng, H. Yu, X. Wang, Y. Xu, H. Wang, L. Wang, Phosphorus-triggered activation of PdPb nanoflowers for enhanced oxygen reduction electrocatalysis, J. Mater. Chem. 10 (2022) 15528.

[S7] Y. Wang, Z. Zhu, K. Xu, W. Guo, T. Yu, M. He, W. Wei, T. Yang, Palladium nanobelts with expanded lattice spacing for electrochemical oxygen reduction in alkaline media, ACS Appl. Nano Mater. 4 (2021) 2118−2125.

[S8] S. Sarkar, S. D. Ramarao, T. Das, R. Das, C. P. Vinod, S. Chakraborty, S. C. Peter, Unveiling the roles of lattice strain and descriptor species on Pt-like oxygen reduction activity in Pd−Bi catalysts, ACS Catal. 11 (2021) 800−808.

[S9] H. Wang, H. Ren, S. Liu, K. Deng, H. Yu, Y. Xu, X. Li, Z. Wang, L. Wang, Bimetallic PdY nanosponges for enhanced oxygen reduction electrocatalysis Nanotechnology 34 (2023) 285402

[S10] D-Y Wei, G-N Xing, H-Q Chen, X-Q Xie, H-M Huang, J-C Dong, J-H Tian, H Zhang, J-F Li, Palladium atomic layers coated on ultrafine gold nanowires boost oxygen reduction reaction Journal of Colloid and Interface Science 650 (2023) 1518–1524

[S11] H. Zhang, X. Li, Y. Wang, K. Deng, H. Yu, Y. Xu, H. Wang, Z. Wang, L. Wang, Porous PdZn bimetallene for oxygen reduction electrolysis, Applied Catalysis B: Environmental, 338 (2023) 123006

Table S3: Comparison of PdY/NCNTs with recently reported Pd-based catalysts in respect to the EOR performance.

Materials	**Electrolyte**	**E_0 (V vs. RHE)**	**ECSA (m^2 g^{-1})**	**j_f/j_b**	**MA (mA mg_{Pd}^{-1}) @ j_f**	**Refs.**
PdY/NCNTs	1 M KOH	0.4	58	1.21	2902	This work
$Sn_{18}Pd_{82}$ alloy	1 M KOH	-	69	1.04	3800	[S1]2023
Pd@N,P,S-3DG	1 M KOH	-	50.3	1.18	1510	[S2]2023
Pd/BNCF-800	1 M KOH	0.605	25.75	0.93	1990	[S3]2022
$Pd_{12}/Ru_3/Ni_3(OH)_2$	1 M KOH	0.65	84.6	0.7	3724	[S4]2022
Pd_8Bi NPs	1 M KOH	0.46	63.8	3.6	2020	[S5]2022
Pd NPs@Ni SAC	1 M KOH	0.41	85	1.1	1093	[S6]2022
$Au@Pd_{0.1}/C$	1 M KOH	0.51	46.2	0.64	1185	[S7]2021
L-Pd aerogel	1 M KOH	0.37	51.3	0.77	2310	[S8]2021
Pd-SnO_2-CSS	1 M KOH	0.58*	22.8	0.67	-	[S9]2023
PbNiBi/rGO	1 M KOH	0.23	4.55	1.23	-	[S10]2023
Pd-Pb CNCs	1 M KOH	0.43	51.70	1.34	4010	[S11]2024

*vs. (SCE)

References

[S1] D. Liu, S. Tian, Y. Zhang, C. Hu, H. Liu, D. Chen, Lin Xu, J. Yang, Ultrafine SnPd nanoalloys promise high-efficiency electrocatalysis for ethanol oxidation and oxygen reduction, ACS Appl. Energy Mater. 2023, 6, 1459−1466.

[S2] C. Karaman, Engineering of N,P,S-Triple doped 3-dimensional graphene architecture: Catalyst-support for “surface-clean” Pd nanoparticles to boost the electrocatalysis of ethanol oxidation reaction, Int. J. Hydrogen Energy 48 (2023) 6691–6701.

[S3] Y. Su C. Li L. Xu J. Xue W. Yuan C. Yao J. Liu M. Cheng , Palladium nanoparticles supported on flower-like boron, nitrogen doped carbon for electrochemical oxidation ethanol reaction, J Alloys Compd 901 (2022) 163333.

[S4] A. Pei, G. Li, L. Zhu, Z. Huang, J. Ye, Y-C Chang, S. M. Osman, C. W. Pao, Q. Gao, B. H. Chen, R. Luque, Nickel hydroxide-supported Ru single atoms and Pd nanoclusters for enhanced electrocatalytic hydrogen evolution and ethanol oxidation, Adv. Funct. Mater. 2022, 32, 2208587.

[S5] X. Lao, M. Yang, X. Sheng, J. Sun, Y. Wang, D. Zheng, M. Pang, A. Fu, H. Li, P. Guo, Monodisperse PdBi Nanoparticles with a Face-Centered Cubic Structure for Highly Efficient Ethanol Oxidation, ACS Appl. Energy Mater. 2022, 5, 1282−1290.

[S6] S. Li, A. Guan, H. Wang, Y. Yan, H. Huang, C. Jing, L. Zhang, L. Zhang, G. Zheng, Hybrid palladium nanoparticles and nickel single atom catalysts for efficient electrocatalytic ethanol oxidation, J. Mater. Chem. A 10 (2022) 6129–6133.

[S7] J. G. Ruiz-Montoya, L. M. S. Nunes, A. M. Baena-Moncada, G. Tremiliosi-Filho, J. C. Morales-Gomero, Effect of palladium on gold in core-shell catalyst for electrooxidation of ethanol in alkaline medium, Int. J. Hydrogen Energy 46 (2021) 23670−23681.

[S8] R. Zhang, L. Zhu, X. Liu, J. Zhu, Y. Zhao, Laser-Assisted Synthesis of Pd Aerogel with Compressive Strain for Boosting Formate and Ethanol Electrooxidation, ACS Sustainable Chem. Eng. 2021, 9, 7837−7845.

[S9] An ionic liquid-present hydrothermal method for preparing hawthorn sherry ball shaped palladium (Pd)-based composite catalysts for ethanol oxidation reaction (EOR), International Journal of Hydrogen Energy, 45, (2020) 1930-1939

[S10] S. Wolf, M. Roschger, B. Genorio, N. Hodnik, M. Gatalo, F. Ruiz-Zepeda, V. Hacker, Reduced graphene oxide as efficient carbon support for Pd-based ethanol oxidation catalysts in alkaline media J. Electrochem. Sci. Eng. 13 (2023) 771-782

[S11] Y. Jin, J. Chen, R. Li, J. Chen, J. Wang, T. Huang, X. Zhang, G. Du, K. Cao, B. Liao, Y. Li, J. Su, F. Xu, N. Wang, Y. Wang, X. Luo, J. Wang, W. Ma, Modulating the exposed facets of Pd-Pb intermetallic compounds via morphology engineering for efficient multifunctional electrocatalysts Applied Surface Science, 648, (2024) 159093.